Chapter 4

End point tagger (EPT)

In the following sections the development of the new end point tagger (EPT) is described.

4.1 Spectrometer magnet

With an incident electron beam energy of $1.604 GeV$ and the η' production threshold of $1.4466 GeV$ only the last $160 MeV$ need to be detected. The detecion range should start a few MeV lower to cover the threshold, we have chosen $170 MeV$. The installed Glasgow-Tagger is still needed to bend the main beam, that do not emit bremsstrahlung, to the beam dump. So the new end point tagger need to be placed in front of the Glasgow-Tagger. One development topic is to keep the deviation of the main beam as minimal as possible, otherwise one can not use the existing beam line in the Glasgow-Tagger. Unfortunately this could only be achieved with a small correction magnet between both spectrometer magnets. A detailed investigation of the magnet parameters and position was done by Leyla Karolin Akasoy in 2008

[156]. Figure 4.1 and 4.2 show the chosen magnet shape and position and its measured field map.

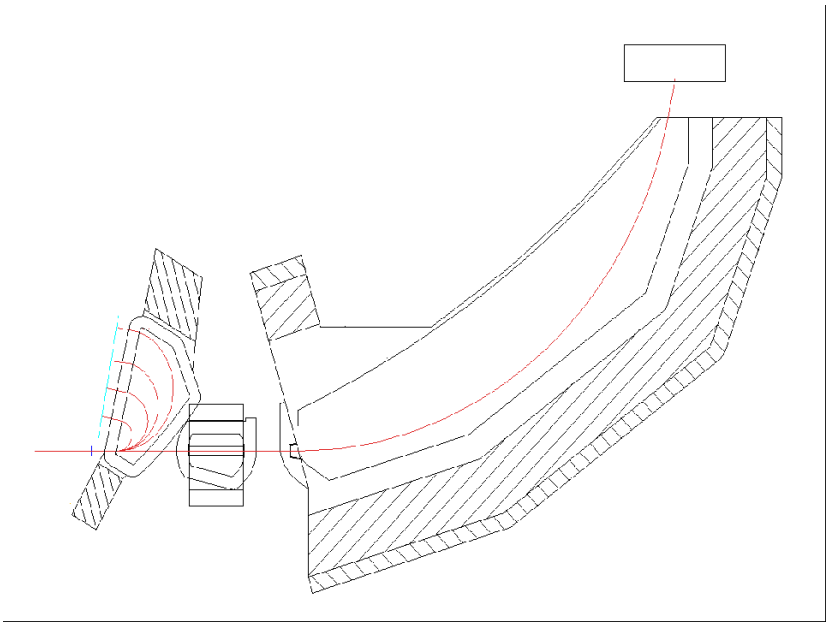

Figure 4.1: Experimental setup with end point tagger (EPT). Following the beam in red entering from left one can see the EPT, the correction magnet, the Glasgow-Tagger and the beam dump.

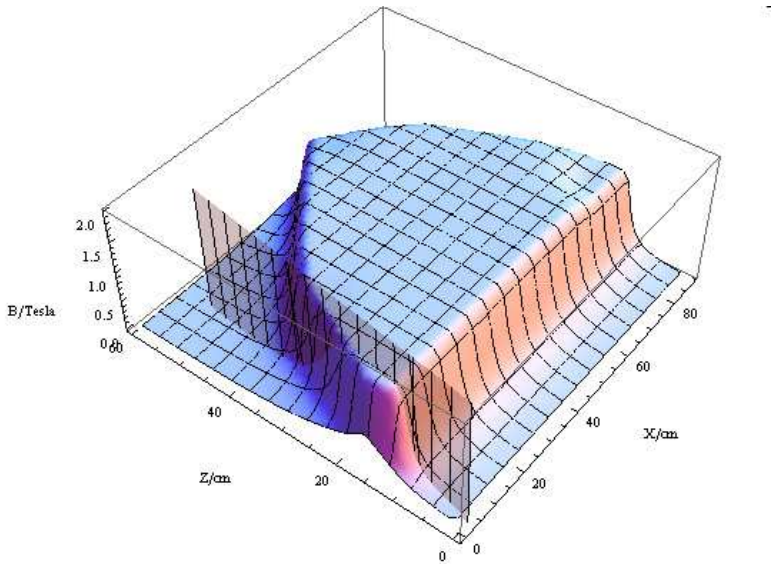

Figure 4.2: Measured field map in the plane of symmetry of the dipole with a grid size of $11.1mm$. The vertical plane indicates the path of the main beam, not emitting any bremsstrahlung.

Ray tracing

To simulate the electron path through the field a ray tracing algorithm was used, mainly based on RAYTRACE from S. Kowalski and H.A. Enge[157], a program that was also used to design MAMI.

The flux density is extrapolated around the given value in vertical direction $B_y^{map}(x,z)$ from the field map with Taylor expansion.

$$B_x(x,y,z) = y\frac{\partial}{\partial y}B_x^{map}(x,z) + \frac{y^3}{6}\frac{\partial^3}{\partial y^3}B_x^{map}(x,z)$$
$$B_y(x,y,z) = B_y^{map}(x,z) + \frac{y^2}{2}\frac{\partial^2}{\partial y^2}B_y^{map}(x,z)$$
$$B_z(x,y,z) = y\frac{\partial}{\partial y}B_z^{map}(x,z) + \frac{y^3}{6}\frac{\partial^3}{\partial y^3}B_z^{map}(x,z)$$

Z is pointing downstream, x is the horizontal component and y the vertical. Due to symmetry only B_x and B_z contain only odd parameters and B_y only even. The derivatives appearing in these equations are all computed by the use of Maxwell's equations converting derivatives of the kind $\left(\frac{\partial^{i+j}}{\partial x^i \partial x^j} B_y^{map}(x,z)\right)_{y=0}$ in the desired form. To get the derivatives of $B_y^{map}(x,z)$ a 5x5 grid of the nearest points in field map was used to fit eq 4.1.

$$\sum_i^3 \sum_j^3 a_{ij} x^i z^j \qquad i+j<3 \tag{4.1}$$

Now it is possible to simulate an electron in all 3 dimensions. The algorithm moves the electron along its flight direction for $\frac{1}{10}$ of the field map grid size and calculates the mean of start and end flux density. Using this a new end point is calculated with bending using simple geometry.

$$r = \frac{p}{eB} \tag{4.2}$$

this is done iteratively until the end point is not changing anymore. For this simulation Mathematica 6 was used.

4.1.1 Dispersion

One of the main design parameters is the dispersion.

$$r = \frac{p}{eB} \tag{4.3}$$

The usable space restricts the focal plane detector ladder to $\approx 0.8m$???. That means the highest electron energy, $170MeV$ has to have a bending radius of $\approx 0.45m$. A simulation of the bremsstrahlung process including a ray tracing of the electron path through the magnetic field gives more accurate values, shown in figure 4.3. One can see that a field of $1.4T$, the maximum achievable without major field distortions, is needed.

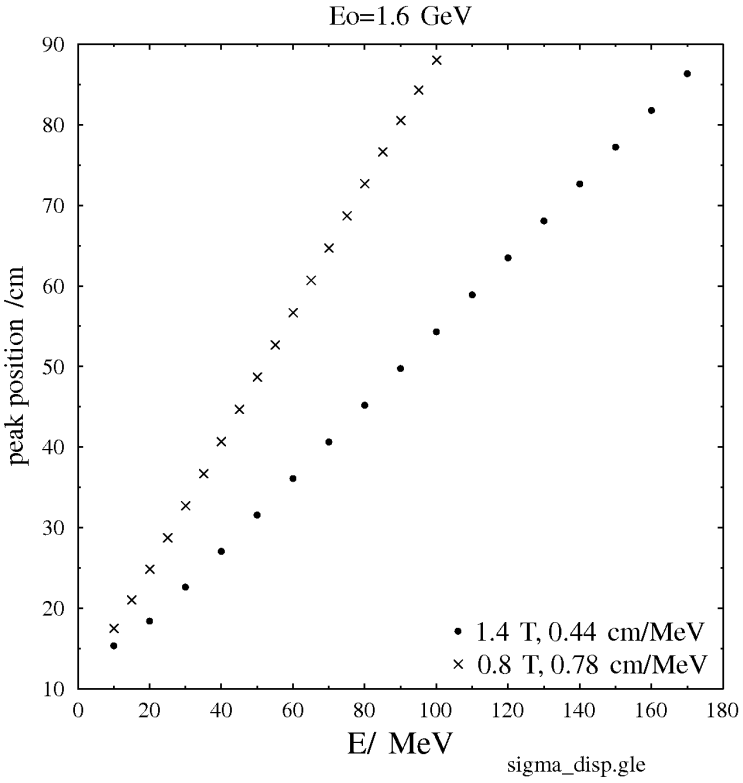

Figure 4.3: Dispersion of the spectrometer magnet, relation between electron energy and bending radius.

4.1.2 Intrinsic resolution estimation

The intrinsic resolution is dictated by bremsstrahlung and its angular distribution. Every transversal component of the emitted photon must be compensated with an equal amount of transversal energy for the electron, like in formula 4.6.

$$E_{\perp_e} = E_e sin(\theta_e) \approx E_e \theta_e \tag{4.4}$$

$$E_{\perp_\gamma} = E_\gamma sin(\theta_\gamma) \approx E_\gamma \theta_\gamma \tag{4.5}$$

$$E_e \theta_e \approx E_\gamma \theta_\gamma \tag{4.6}$$

$$\theta_e \approx \left(\frac{E_\gamma}{E_e} - 1\right) \theta_\gamma \tag{4.7}$$

$$\theta_e \propto \frac{1}{E_e} \tag{4.8}$$

The proportionality in 4.8 is not related to the angular distribution function, it follows simple dynamic rules. For sure, other parameters, like the angular distribution of the incoming electron beam, have an impact on the resolution, but this are external (not intrinsic) parameters.

Again, the absolute values have been determined by a simulation of the bremsstrahlung process including a ray tracing of the electron path through the magnetic field, shown in figure 4.4 and 4.5.

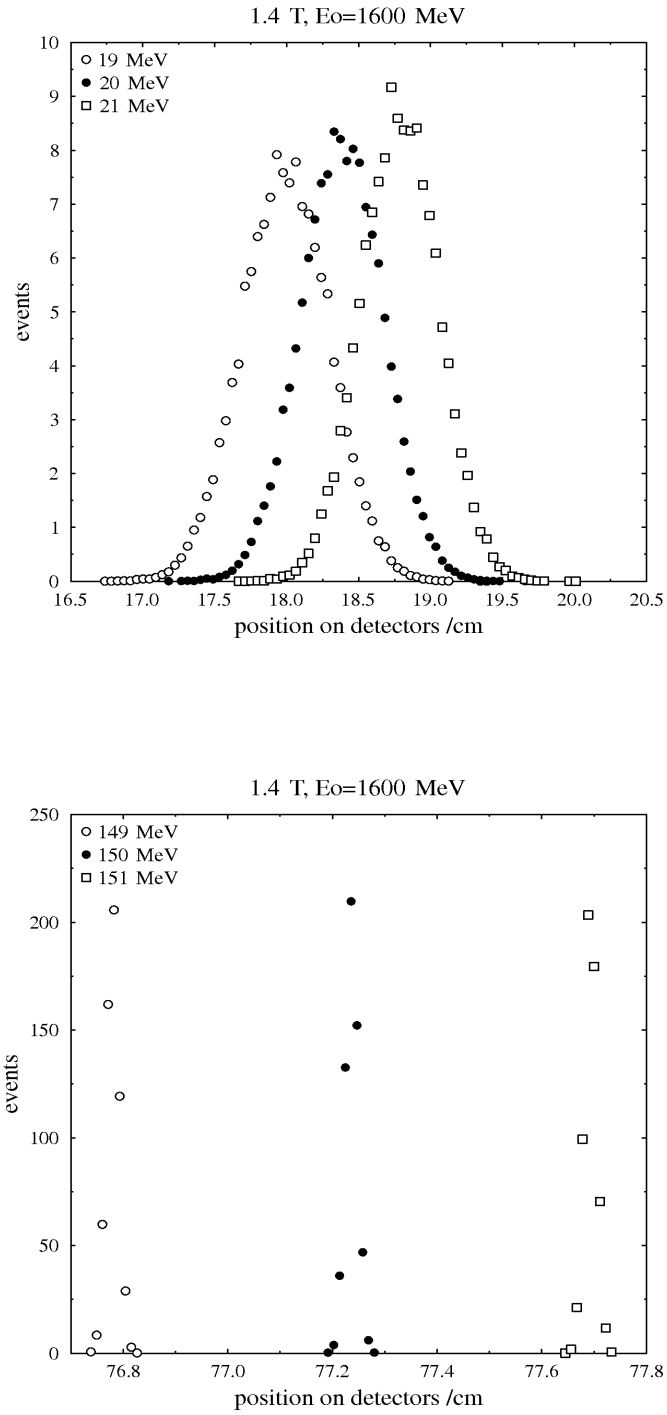

Figure 4.4: Spacial distribution along the focal plane for different electron energies. The width indicates the intrinsic resolution for this energy.

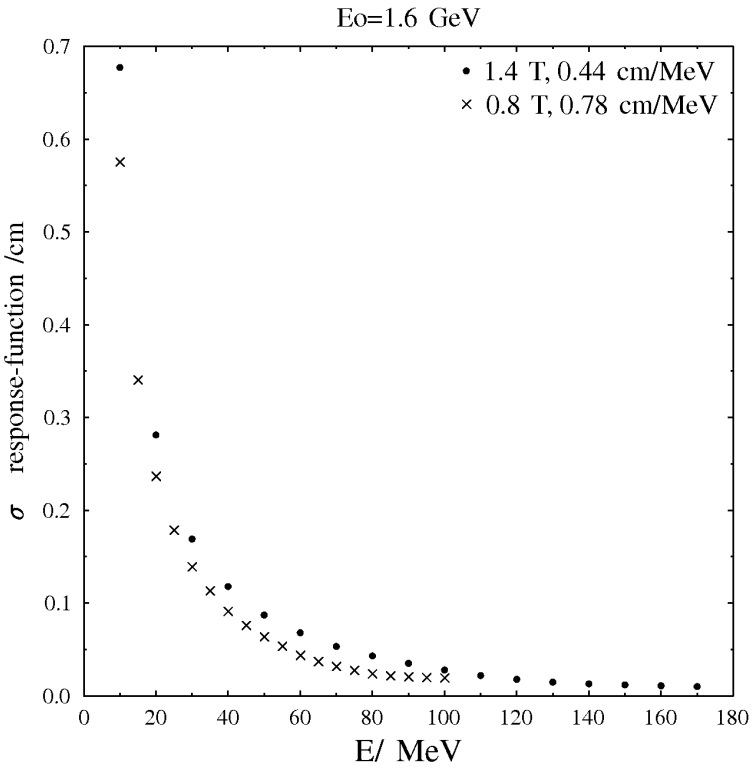

Figure 4.5: Intrinsic resolution for the end point tagger in relation to electron energy.

4.1.3 Distortion of the main beam.

The path length of the main beam through the magnet is as minimal as possible, to minimize the bending. Never the less the beam is bended by $\approx 3.5°$. Another issue is the horizontal output angle of $\approx 70°$. This will cause a strong vertical divergence of the main beam. To investigate the beam optics, a ray trace simulation was done for horizontal and vertical orientation.

Horizontal

Using the existing Glasgow-Tagger to dump the main beam is the main issue in the horizontal orientation. In the following fig. 4.6 one can see the horizontal offset related to the not bended beam along the traveled path.

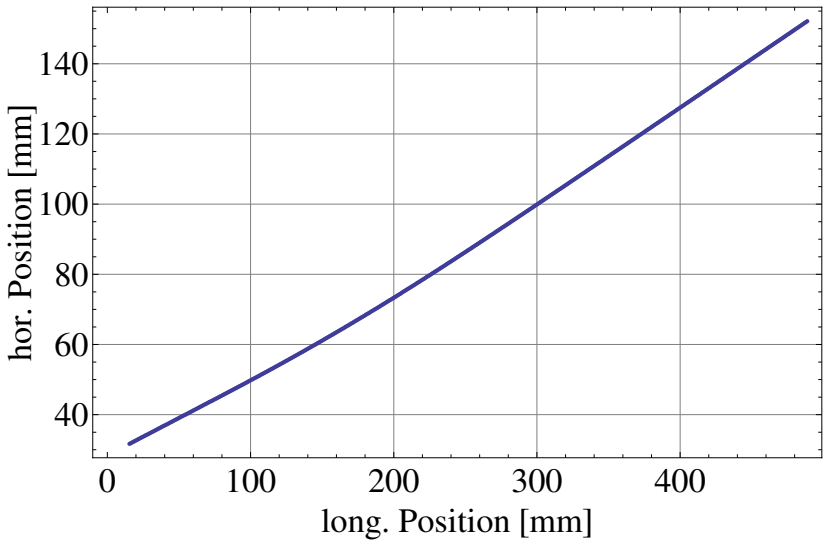

Figure 4.6: Main beam path along xz-plane. As desired there is only a small bending,

The offset is unproblematic but the deviation of the angle showed in fig 4.7 needs a compensation. As one can see the horizontal angle is changed by $\approx 3,5°$.

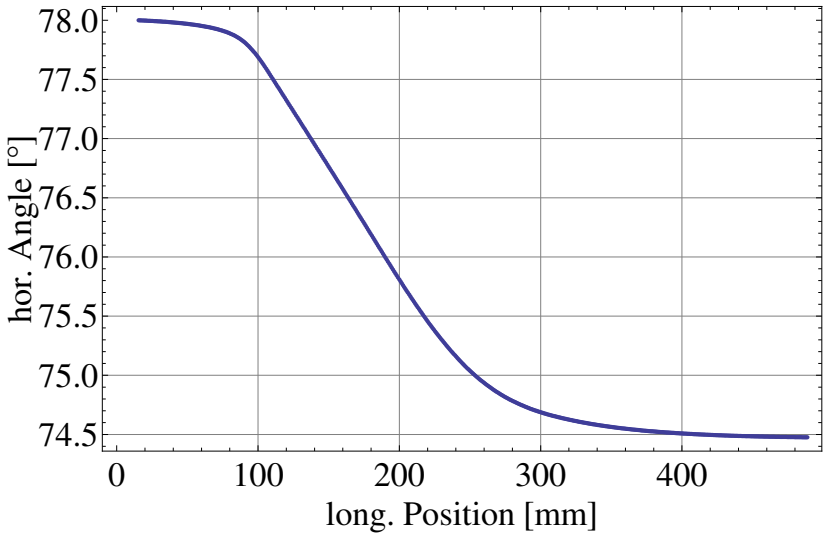

Figure 4.7: Angle of the electron main beam in relation to the exit dipole edge.

Without an compensation this will lead to an offset of $6\frac{cm}{m}$ related to the existing beam line. The beam dump is positioned $10,9m$ downstream the EPT, without correction we miss the dump by $0.654m$. Therefore a correction magnet is needed.

Vertical

In the vertical orientation there is no bending, but never the less also in this orientation the EPT has influence on the beam. If the beam direction is not perpendicular to the dipole edge it will be vertical defocused (fig 4.8).

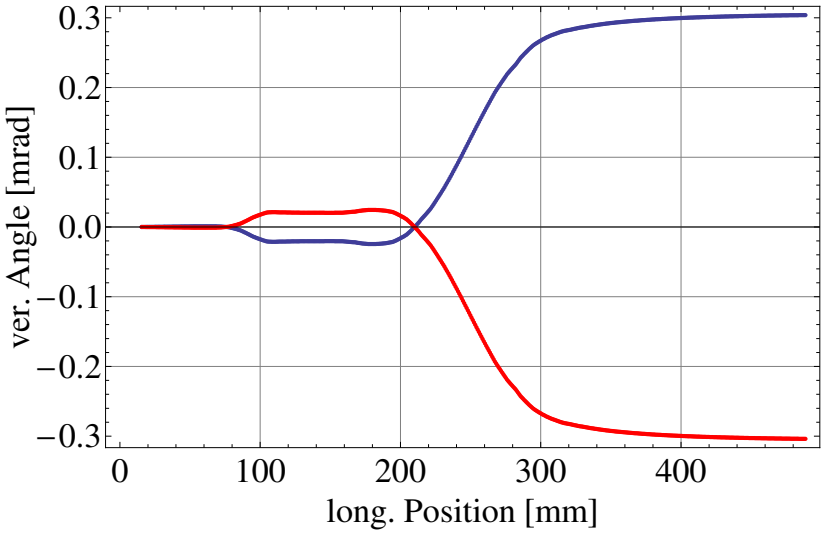

Figure 4.8: Vertical deviation angle from desired path for incoming electron with $0.5mm$ vertical position offset. Blue shows positive offset, red is negative

For an incoming electron with $0.5mm$ vertical position offset the deviation at the beam dump positioned $10,9m$ downstream is $3.27mm$ which is small enough to still hit the dump. The incident electron beam from MAMI has a usual width of $\approx 300\mu m$. At the dump this results in an unproblematic width of only $2.18mm$.

4.1.4 Correction magnet.

Fortunately the chosen correction dipole has a nearly the same dispersion like the EPT. Therefor both magnets are connected in series to the power supply. It is not necessary to compensate the EPT accurate, a small rest bending can be compensated by MAMI with changing the incident beam.

TODO: jÃijrgen wegen Bilder und daten des magneten fragen

Fig 4.9 shows the horizontal deviation from the desired path with correction magnet along the way to the beam dump. Also the bottlenecks are shown.

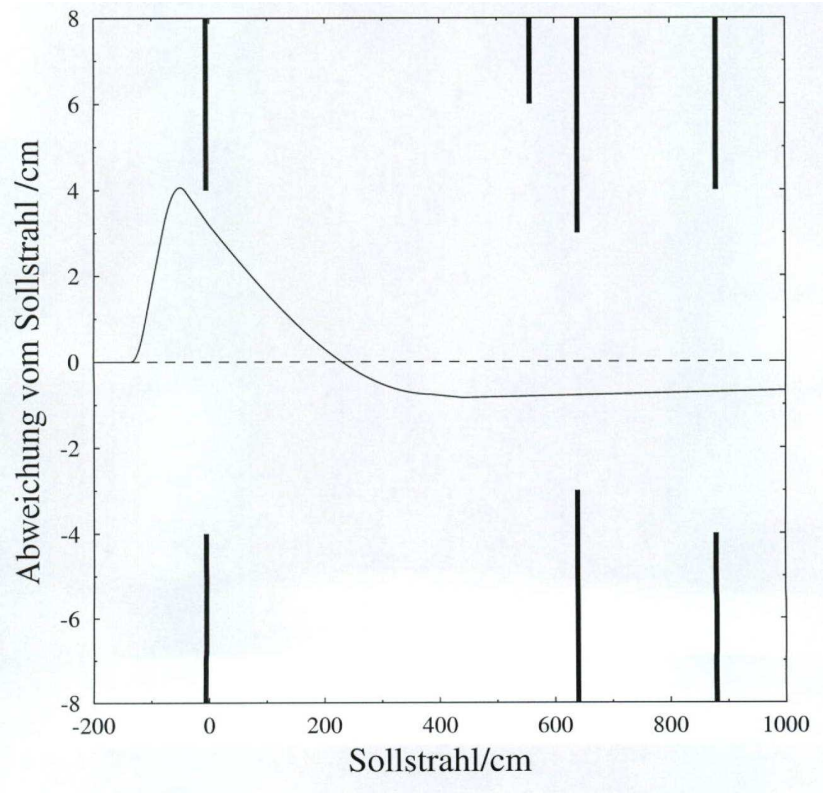

Figure 4.9: Horizontal deviation from the desired path with correction magnet along the way to the beam dump. The black lines represent the bottlenecks along the path. The first black lines show the Glasgow-Tagger entrance, the next small line NMR-probe, then the Glasgow-Tagger exit and the dump entrance.

4.1.5 Readout Electronic.

First the PMT signal is feaded in 3 16 channel LeCroy???? amplifiers, which increase the signal by a factor of ten. It is also used as impedance converter, cause the signal will be split passively in two signals. One of this analog signals is used as input for a 96 channel FASTBUS QDC.

TODO: FASTBUS Unterlagen -¿ electronic

The other one is connected to a 3 16 channel LeCROY???? CFD. The digital discriminator output is used as stop for a 64 channel Catch TDC, which is started by the experiment trigger.

Figure 4.10: Schematic overview of the read out electronics.

ADC

The QDC is the slowest part in the read out, but fortunately it is needed only one time to adjust the HV in a way that all signal heights are similar and to set a reasonable CFD threshold for all 47 PMT's. This is shown in fig 4.12, in this plot the discriminator threshold for the TDC's is positined around QDC channel 700.

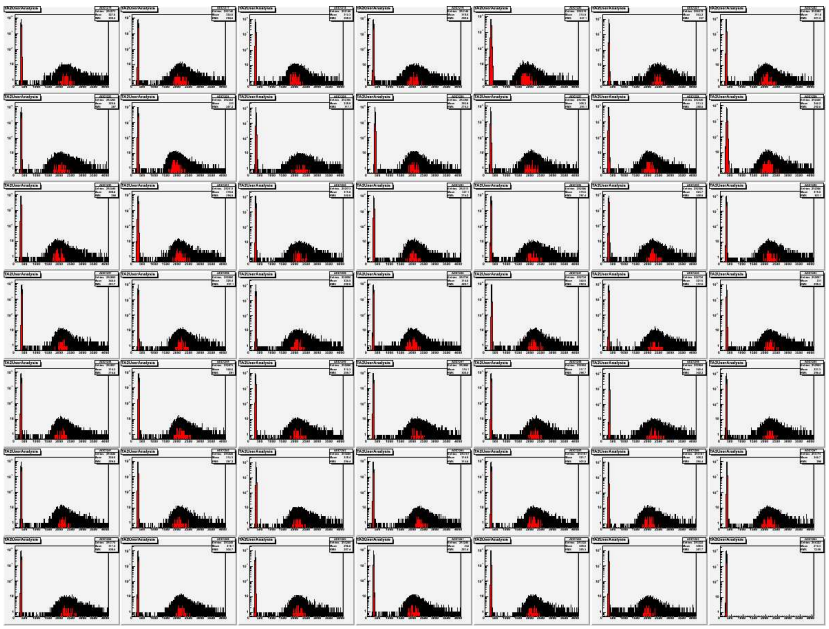

Figure 4.11: QDC readout for all 47 EPT channels. The signal position was adjusted around QDC channel 2000.

TDC

After calibrating the HV and the thresholds of the CFD only timing information is needed.

TODO: find a better Plot without dip after peak

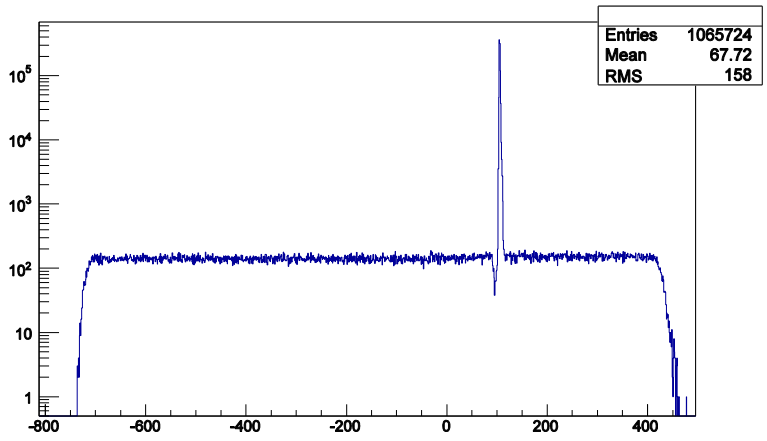

Figure 4.12: QDC readout for all 47 EPT channels. The signal position was adjusted around QDC channel 2000.